Supporting Information for

Advancement in Liquid Exfoliation of Graphite through Simultaneously Oxidizing and Ultrasonicating

*Ge Shi[a,b], Andrew Michelmore[b], Jian Jin[c], Luhua Li[d], Ying Chen[d], Lianzhou Wang[e], Hua Yu[e], Gordon Wallace[f], Sanjeev Gambhir[f], Shenmin Zhu[g], Pejman Hojati-Talemi[b], Jun Ma[*a,b]*

[a]School of Engineering and [2]Mawson Institute, University of South Australia, SA5095, Australia

[b]Suzhou Institute of Nano-Tech and Nano-Bionics, Chinese Academy of Sciences, Suzhou 215123, China

[c]Institute for Frontier Materials, Deakin University, Geelong Waurn Ponds Campus, VIC 3216, Australia

[d]School of Chemical Engineering and AIBN, the University of Queensland, QLD 4072, Australia

[e]Intelligent Polymer Research Institute, University of Wollongong, NSW 2500, Australia

[f]State Key Laboratory of Metal Matrix Composites, Shanghai Jiao Tong University, 200240, China

[g]State Key Laboratory of Metal Matrix Composites, Shanghai Jiao Tong University, 200240, China

1. Experimental setup for oxidi-sonication

Graphite particles were first mixed with acids and potassium permanganate as shown in the Experiment, and then the mixture was immediately placed into an ultrasonication bath to simultaneously undertake oxidation and ultrasonication (oxidi-sonication), as shown in Figure S1.

Fig. S1 Ultrasonication bath for simultaneously oxidizing and ultrasonicating graphite (oxidi-sonication)

2. Comparison of our oxidi-sonication method with the improved Hummer's method[1]

In the oxidi-sonication, the acid mixture consists of 26 g phosphoric acid, 6 g sulphuric acid and 0.1 g graphite. After 0.4 g potassium permanganate was added, Mn_2O_7 formed at a low speed which is due to phosphoric acid used. The temperature arose slowly and the colour changed to red purple owing to the dissolution of Mn_2O_7 (Figure S2 a1). The reaction rate was low, so some potassium permanganate particles left at the beaker bottom (Figure S2 a2).

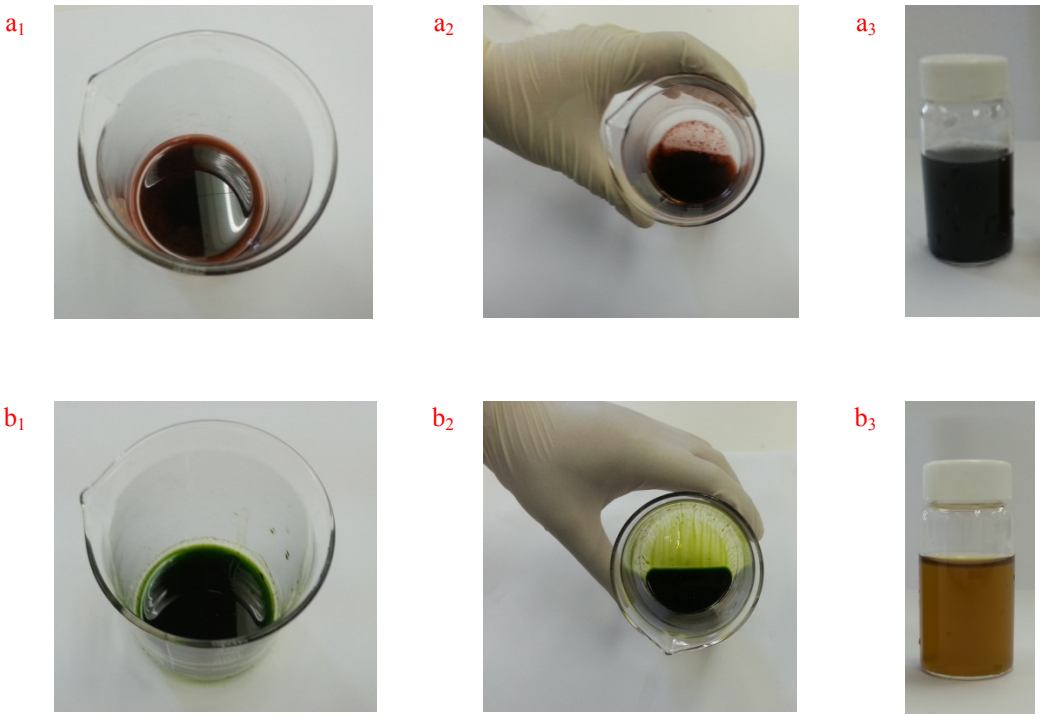

Fig. S2 Comparison between our oxidi-sonication method (a) and the improved Hummer's method (b).

In the improved Hummer's method, the precursor consists of 0.76 g phosphoric acid, 6.5 g sulphuric acid and 0.1 g graphite. Following the addition of potassium permanganate (0.6 g), Mn_2O_7 formed immediately (Figure S2 b1) as far less phosphoric acid used. Temperature increased rapidly to 40–50°C, the mixture turned to yellow green, and most of potassium permanganate particles reacted with acids (Figure S2 b2).

After 1-hour treatment, the improved Hummer's method oxidized graphite excessively, resulting in yellow colour graphene oxide. By contrast, the oxidi-sonication method oxidized graphite gently implying a low degree of oxidation. The difference is shown in Figures S2 a3 and b3.

3. AFM micrographs of oxidi-sonication graphene sheets

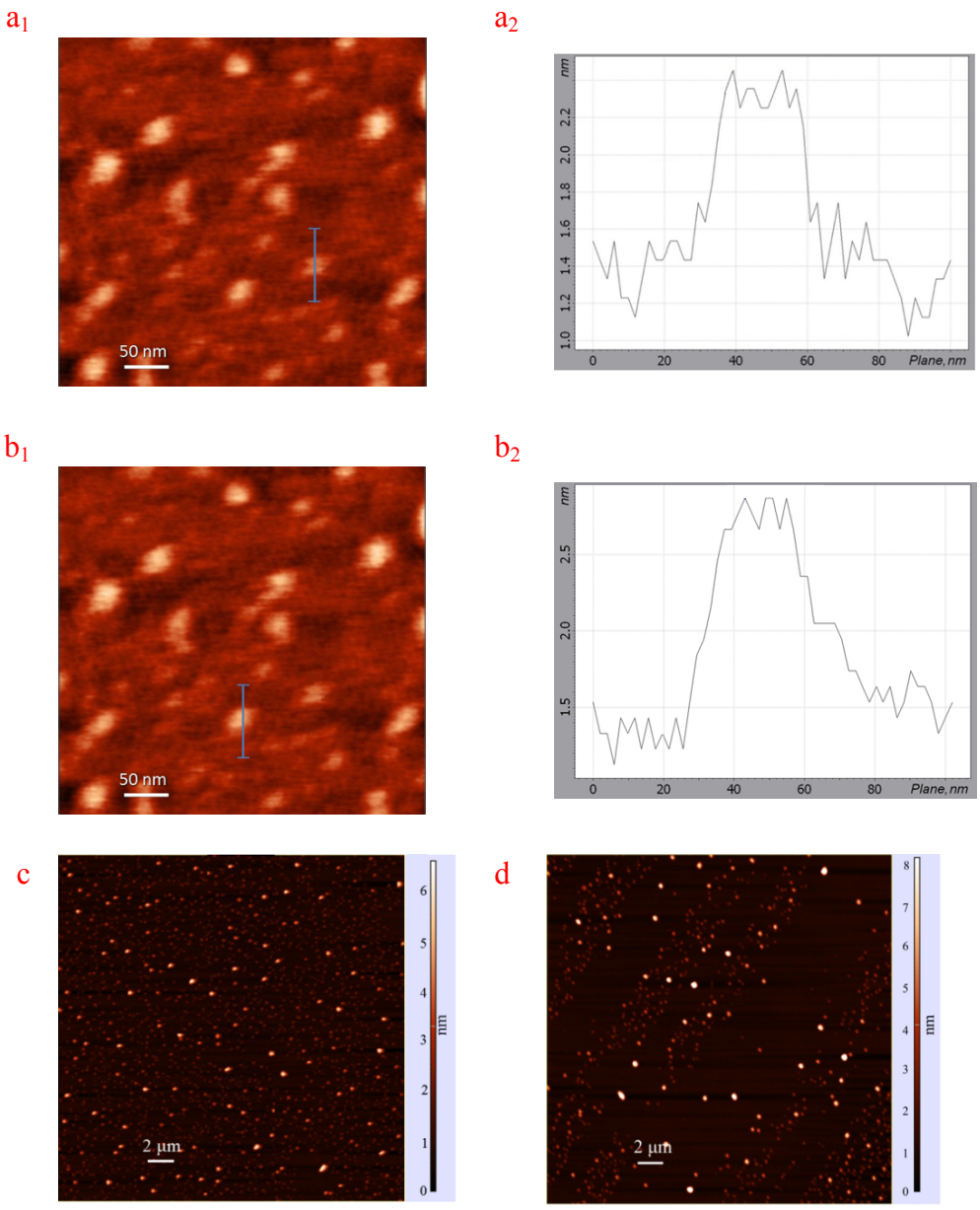

Fig. S3 AFM micrographs and height profiles of graphene sheets fabricated by 60 min oxidi-sonication

Figs. S3 a_1 and a_2 contain the high magnification AFM images and height profiles of the 60 min oxidi-sonication graphene sheets. All these show the thicknesses at around 1 nm. In low magnification AFM images (Fig. S3 c and d), most oxidi-sonication graphene sheets are 1–6 nm in thickness and 50–200 nm in lateral dimension.

4. Acidic functionalities of our graphene sheets

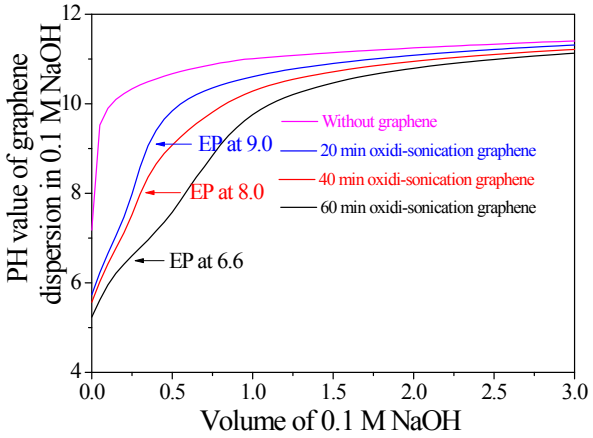

Fig. S4 Titration of graphene suspension using 80 mg graphene sheets (on dry basis) at different time intervals with 0.1 M NaOH.

Increase in acidic functionality as a function of increasing the oxidi-sonication time of graphite was further observed using the simple acid-base titration of aqueous dispersion of graphene. Ayrat et al. have demonstrated analysing the acid functionalities of GO.[2] Extrapolating similar conditions of titration for analysing and comparing the acidic functionalities in the three graphene dispersion was followed. Three different samples drawn at the intervals of 20, 40 and 60 min were analysed by keeping the identical conditions of analysis. A similar quantity of graphene sheets (equivalent to 80 mg calculated on dry-basis) was taken in a beaker containing Milli-Q water. 0.1 M NaOH solution was incrementally added using Metrohm auto-titrator in 0.05 ml/ dose, and the corresponding pH was recorded automatically. Equivalence point (EP) at pH 7.9 is observed for all three samples and was typically assigned to acidic functionalities arising from graphene oxide.[3] Regarding analysis of the sample treated for 60 min, additional EP at pH 6.6 and 9.0 are also observed and can be assigned to the acidity arising from the phenolic functionalities.[2]

5. TGA of our graphene and graphene oxide

TGA graphs of our graphene samples are compared with that of graphene oxide fabricated according to ref [1]. Graphene oxide shows an obvious mass loss between 50 and 150 °C corresponding to the disappearance of absorbed water molecules. A major weight loss occurs

between 150 and 200 °C referring to the escape of CO and CO_2, both of which were produced from the large number of oxygen-containing functional groups. By contrast, our oxidi-sonication graphene sheets do not have an abrupt weight loss. These results reflect that the oxidi-sonication created a moderate number of functional groups, high thermal stability and sufficient crystalline integrity for graphene.

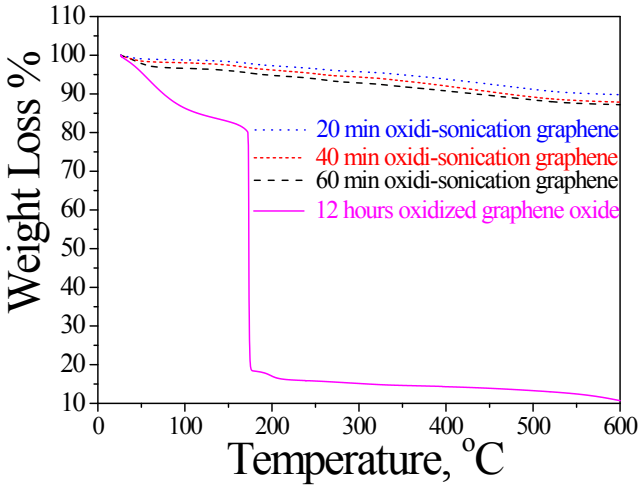

Fig. S5 TGA graphs of graphene sheets fabricated by oxidi-sonication (20, 40 and 60 min) and graphene oxide by oxidation.[1]

6. Fabrication of thin graphene film

Graphene sheets fabricated by the oxidi-sonication can get dispersed in solution via ultrasonication by overcoming the intersheet van der Waals forces through solvation forces and electrostatic force. Solvation forces are the result of restructuring solvent molecules at the liquid/solid boundary due to the interactions between the solid surface and the solvent molecules. Electrostatic force is generated by charged sheet edges due to few functional groups ionized in solution. The oxygen-containing groups of graphene sheets can produce hydrogen bonds between them, with acetone responsible for stabilizing the suspension.[4] Therefore, most graphene sheets should separate from each other at this stage. After the suspension was dropped on pre-coated polystyrene membrane, acetone evaporated quickly and the graphene concentration increased, resulting in an effective decrease in solvent

force.[5] Therefore, the graphene sheets would move closer to each other and form two fundamental interaction geometries: either edge to edge or face to face or both. Because graphene sheets have a low lateral dimension of 50–100 nm and the sheet edges cut by the oxidi-sonication are rich in hydrophilic oxygenated groups, most sheets would connect with each other edge to edge and may form a structure similar to nanoribbons. As acetone evaporates, graphene sheets should deposit on the polystyrene coating through π-π interactions. With further solution casting, there would be more face to face interaction between the deposited graphene sheets, causing island–like assembling. After most graphene sheets deposit on polystyrene substrate, the spin coating applied may separate these islands; that is, spin coating may promote the movement of graphene sheets during the rapid evaporation of acetone with such a high centrifugal force, resulting in relatively homogeneous, interconnected structure.[6]

7. Surface roughness of polystyrene substrate

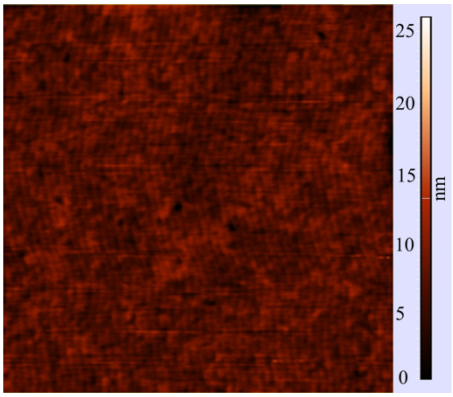

Fig. S6 AFM micrograph of the polystyrene substrate surface.

In Fig. S6, the polystyrene coating on the glass substrate has flat surface with a height of ~15 nm.

8. Surface resistance of graphene thin films

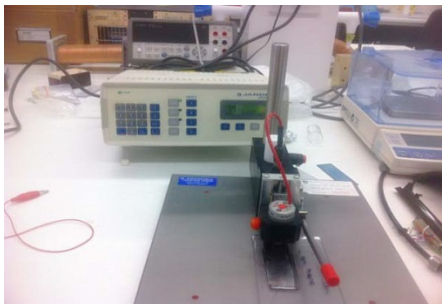

Fig. S7 Four-point probe used to test the surface resistivity (911 Ω/square) of graphene films prepared by casting graphene suspension.

We fabricated thin films by casting graphene solution; a typical film shows a surface resistance of 900±15 Ω/square (Figure S7). The values of surface resistance can be reduced by increasing the film thicknesses.

9. Comparison of optical-electrical properties

To analyze the transmittance and sheet resistance data of transparent conducting films, it is important to note that transparency (T) and sheet resistance (R_s) are in fact linked each other. Both are determined by the response of electrons to either static voltage or dynamic light electric field. The sheet resistance is ultimately controlled by the 3-dimensional DC conductivity, σ_{dc}, via $R_s = (\sigma_{dc}t)^{-1}$, where t is the film thickness. The transmittance is controlled by the optical conductivity σ_{op}, via $T = (1+ \frac{Z_0}{2}\sigma_{op}t)^{-2}$, where Z_0 is the impedance of free space and has the value 377 Ω. The optical conductivity is related to the Lamer-Beer adsorption coefficient α, by $\sigma_{op} \approx 2\alpha/Z_0$.[7]

After combining these equations and eliminating t, the relationship between transparency (T) and sheet resistance (R_s) can be presented as the conductivity ratio, σ_{dc}/σ_{op}, using the equation: $\sigma_{dc}/\sigma_{op} = Z_0/2R_s(T^{-1/2}-1)$ where Z_0 = 377 Ω is the impedance of free space. A high σ_{dc}/σ_{op} value indicates the transparent conductor having high optical-electrical properties.[8] Table S1 list the calculated σ_{dc}/σ_{op}

values for transparent conductors fabricated by various methods. In comparison, our transparent graphene film could have better opt-electrical properties than other films made by (i) spin coating and dip coating of reduced GO and (ii) electrochemically exfoliation of raw graphite.

Table S1 Comparison of our sheet film with previous ones.

Fabrication Methods	Graphene type	Sheet Resistance (Ω/sq)	Transmittance (%)	σ_{dc}/σ_{op}	Reference
Spin coating	Oxidi-sonication	815	86	2.95	Current work
	Thermal reduction of GO	1000	80	1.60	[9]
	Thermal reduction of GO	2700	90	1.3	[10]
Langmuir-Blodegett Deposition	Thermal and Chemical reduction of GO	459	90	7.29	[8]
	Chemical reduction modified GO	8000	83	0.24	[11]
	Chemical reduction of GO	1100	91	3.54	[12]
Vacuum filtration	Chemical reduction of GO	350	80	4.5	[13]
Electrochemically exfoliation	Graphene	2400	73	0.46	[14]
Dip coating	Thermal reduction of GO	1800	70	0.54	[15]
CVD	Ni Substrate	1000	90	3.5	[16]
	Ni Substrate	230	72	4.6	[17]
	Cu Substrate	350	90	9.96	[18]

10. Current–voltage characteristics of graphene films

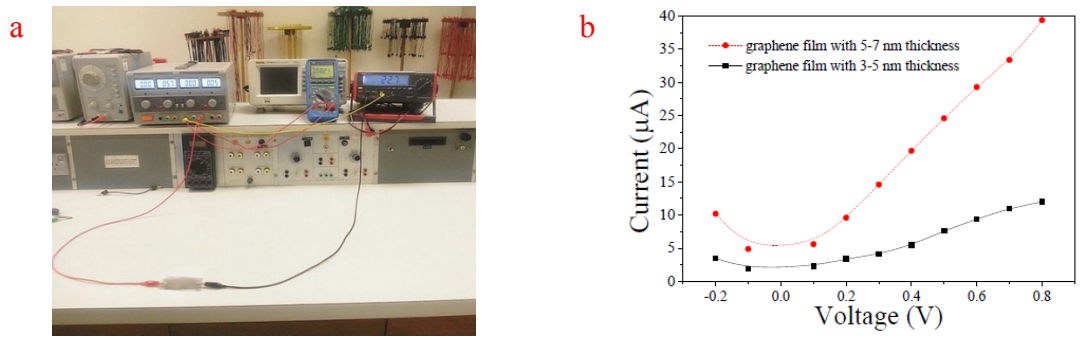

Fig. S8 Current–voltage measurement (a) devices and (b) characteristics

In Fig. S8, the current-voltage measurement indicates that the oxidi-sonication graphene films have high conductivity.

Figure S9 shows an AFM image and its height profile of a graphene sheet made by the oxidi-sonication of 60 min. The image is the same as in Figure 2d, but it measured the height of a relatively large sheet. The height peak demonstrates both flat area and spikes; the latter is most likely caused by either uneven sheet surface or AFM resolution.

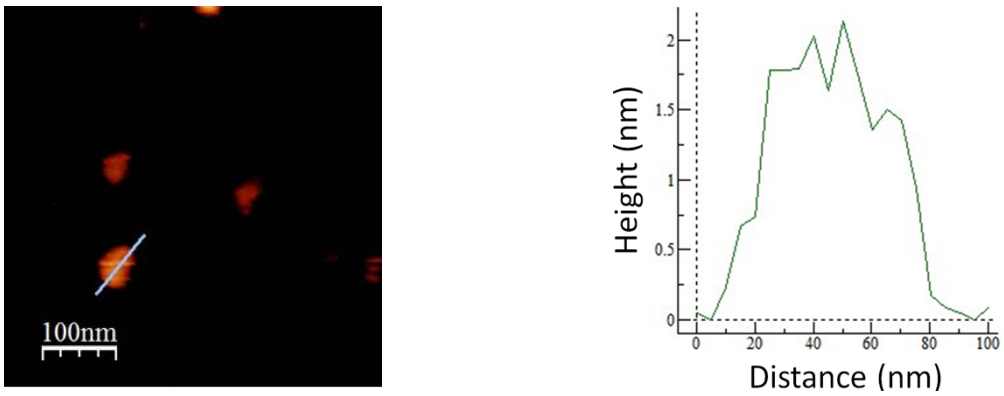

Fig. S9 AFM image and its height profile for graphene sheets made by 60-min oxidi-sonication

References

1. D. C. Marcano, D. V. Kosynkin, J. M. Berlin, A. Sinitskii, Z. Sun, A. Slesarev, L. B. Alemany, W. Lu, J. M. Tour, *ACS Nano*, 2010, **4**, 4806–4814.
2. A. M. Dimiev, L. B. Alemany, J. M. Tour, *ACS Nano* 2012, **7**, 576–588.
3. B. Konkena, S. Vasudevan, *J. Phys. Chem. Lett.* 2012, **3**, 867–872.
4. S. Dubin, S. Gilje, K. Wang, V. C. Tung, K. Cha, A. S. Hall, J. Farrar, R. Varshneya, Y. Yang, R. B. Kaner, *ACS Nano*, 2010, **4**, 3845–3852.
5. C. Cheng, D. Li, *Adv. Mater.* 2013, **25**, 13–29.
6. H. W. Kim, H. W. Yoon, S. M. Yoon, B. M. Yoo, B. K. Ahn, Y. H. Cho, H. J. Shin, H. Yang, U. Paik, S. Kwon, J. Y. Choi, H. B. Park, *Science*. 2013, **342**, 91–95.
7. S. De, J. N. Coleman, *ACS Nano*, 2010, **4**, 2713–2720.
8. Q. Zheng, W. H. Ip, X. Lin, N. Yousefi, K. K. Yeung, Z. Li, J. K. Kim, *ACS Nano*, 2011, 7, 6039–6051.
9. H. A. Becerril, J. Mao, Z. Liu, R. M. Stoltenberg, Z. Bao, Y. Chen, *ACS Nano*, 2008, **2**, 463–470.
10. I. N. Kholmanov, S. H. Domingues, H. Chou, X. Wang, C. Tan, J. Y. Kim, H. Li, R. Piner, A. J. G. Zarbin, R. S. Ruoff. *ACS Nano*. 2013, 7, 1811–1816.
11. X. L. Li, G. Y. Zhang, X. D. Bai, X. M. Sun, X. R. Wang, E. Wang and H. J. Dai, *Nat. Nanotechnol*., 2008, **3**, 538–542.
12. X. Lin, J. Jia, N. Youse, X. Shen and J. K. Kim, *J. Mater. Chem. C*, 2013, **1**, 6869–6877.
13. H. Feng, R. Cheng, X. Zhao, X. Duan and J. Li, *Nat. Commun.*, 2013, **4**, 1539.
14. K. Parvez, R. Li, S. R. Puniredd, Y. Hernandez, F. Hinkel, S. Wang, X. Feng and K. Müllen, *ACS Nano*, 2013, 7, 3598–3606.
15. X. Wang, L. Zhi, K. M$\ddot{u}$llen. *Nano Lett.*, 2008, **8**, 323–327.
16. A. Reina, X. Jia, J. Ho, D. Nezich, H. Son, V. Bululovic, M. S. Dresselhaus, J. Kong, *Nano Lett.,* 2009*,* **9**, 30–35.
17. L. G. D. Arco, Y. Zhang, C. W. Shlenker, K. Ryu, M. E. Thompson, C. Zhou, *ACS Nano.,* 2010**, 4**, 2865–2873.
18. X. Li, Y. Zhu, W. Cai, M. Borysiak, B. Han, D. Chen, Richard. D. Piner, L. Colombo, R. S. Ruoff, *Nano Lett*., 2009, **9**, 4359–4363.